LANGMUIR Article
Cite This: Langmuir 2019, 35, 4626−4633
pubs.acs.org/Langmuir

One-Step Preparation Method of Flexible Metafilms on the Water−Oil Interface: Self-Assembly Surface Plasmon Structures for Surface-Enhanced Raman Scattering Detection

Nan Yang, Tingting You,* Yukun Gao, Sichen Lu, and Penggang Yin*

Key Laboratory of Bio-Inspired Smart Interfacial Science and Technology of Ministry of Education, School of Chemistry, Beihang University, No. 37 Xueyuan Road, Haidian District, Beijing 100191, China

Supporting Information

ABSTRACT: The present study demonstrated a one-step method for the first time to fabricate self-assembled gold nanoparticle (AuNP) metafilms at the water−toluene interface by adding polystyrene−polyisoprene−polystyrene as the support layer. The thiolated polyethylene glycol and ethanol were used to tune the surface charge density on the AuNPs, constructing a balanced situation at the water−toluene interface. The flexible (AuNP) metafilm can be easily obtained after evaporation of the toluene phase and further used as a surface-enhanced Raman scattering (SERS) substrate for trace thiram detection. The SERS sensitivity was tested using standard Raman probes such as crystal violet and malachite green, both with the detect concentration reaching 1×10^{-11} M. Moreover, the excellent reproducibility and elastic properties make the metafilm promising in practical detection. Hence, the trace thiram detection on an orange pericarp was inspected with the detection limit of 0.5 ppm (1×10^{-6} M) as well as a favorable linearity relation with a correlation coefficient of 0.979, exactly matching the realistic application requirements.

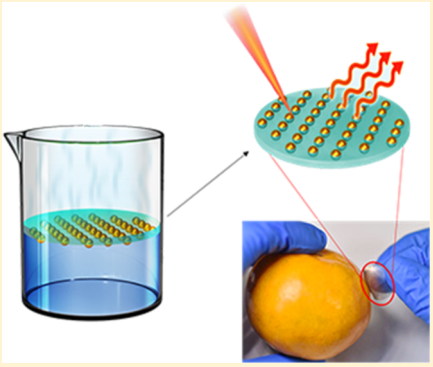

INTRODUCTION

In recent years, there has been an increasing interest in self-assembled nanoparticle (NP) structures.[1,2] Self-assembled nanostructure films have emerged as powerful platforms in surface-enhanced Raman scattering (SERS), catalysis, sensor science, and biomaterials research areas.[3−6] Numerous studies have explored the methods of fabricating ordered assembled arrays such as Langmuir−Blodgett technique,[7−10] nanolithography,[11,12] electrophoretic deposition,[13] and interfacial assembly (air−liquid, liquid−liquid and liquid−gas−solid interface).[3,4,14−16] Self-assembly of NPs at liquid−liquid interfaces was found to be a highly effective and low-cost way to form uniform arrays among these methods. The NPs at the liquid−liquid interface are stabilized under the interparticle interactions which are governed by electrostatic repulsion, steric hindrance, hydrophobic interaction, and van der Waals forces.[1,15,17] Previous studies indicated that the assembly of NPs at the interface is introduced by a minimization of the Helmholtz free energy.[18,19] Moreover, the key issue to form assembled nanostructures at the water−oil interface is to reduce the surface charge density of metal NPs using an appropriate surfactant such as alkylthiol.[2,3,15,20] Besides surfactants, some solvent that is soluble in both water and oil such as ethanol, acetone, and isopropanol were also used to adjust the interfacial energy and polarity of the solution to help fabricate assembled nanostructures at the water−oil interface.[17,21]

The self-assembly process of metal NPs can create 1−10 nm interparticle distances which is called "hotspots" in SERS.[17,22] These uniform nanogaps between metal NPs could generate strong coupling effect of the local electromagnetic field.[23] The excitation of localized surface plasmon resonance between coupled NPs arises intense field enhancement, resulting in the dominated electromagnetic enhancement of SERS.[23]

SERS is an important tool in analytical chemistry, food safety, environment monitoring, and biological application because of the attractive feature of nondestructive examination.[23−33] There are two general methods to utilize the liquid−liquid interface-assembled metal NP films as the SERS substrate. The indirect method is to transfer the assembled nanostructures onto a hard substrate such as Si wafer, glass slide, and copper grids through a horizontal deposition or vertical retraction of the immersed substrate procedure.[2−4,14,15] It is inevitable that random aggregates, multilayer structure, and voids might be induced during the transferring steps.[34] To overcome this shortcoming, Liu's group reported a method by collecting the SERS signal from the liquid interfacial directly, and this liquid interfacial SERS platform showed great potential in the multiphase detection.[34,35] However, using the self-assembled metal NP films as the flexible SERS

Received: December 23, 2018
Revised: January 22, 2019
Published: March 20, 2019

DOI: 10.1021/acs.langmuir.8b04271
Langmuir 2019, 35, 4626−4633

Scheme 1. Schematic Diagram of the One-Step Self-Assembly of the AuNP Metafilm

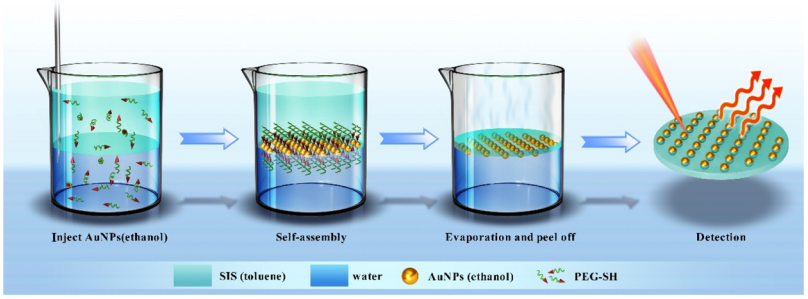

substrate directly is extremely desired for practical application on nonplanar objects.

This paper reported a one-step method for the first time to fabricate a flexible self-assembled gold NP (AuNP) metafilm at the water−oil interface, which can be used for SERS detection. In this work, AuNPs were dispersed in ethanol and injected in the water−toluene interface, and the aggregations were formed immediately with the help of thiolated polyethylene glycol (PEG-SH). It is noticed that the polystyrene−polyisoprene−polystyrene (SIS) molecule was added to the toluene phase, and worked as a support layer after an evaporation process of toluene. The self-assembled AuNP metafilm exhibits excellent SERS performance with the lowest detection concentration of CV (crystal violet) and MG (malachite green) of about 1×10^{-11} M. Practical examination of thiram detection on an orange pericarp was carried out with a lowest detection concentration of 1×10^{-6} M (0.5 ppm), which is far below the National Standard of China (GB) of 1×10^{-5} M (5 ppm). A favorable linearity relation was achieved between 1000 and 0.5 ppm with a correlation coefficient of 0.979 at the 1372 cm^{-1} peak. Therefore, this study makes a major contribution to research on the one-step fabrication of the self-assembled AuNP metafilm, which indicates a promising SERS substrate on food safety and pesticide residue detection.

EXPERIMENTAL SECTION

Reagents. Chloroauric acid ($HAuCl_4$) and polystyrene-*block*-polyisoprene-*block*-polystyrene (SIS, styrene 17 wt %) were purchased from Sigma-Aldrich (Shanghai, China). Sodium citrate ($C_6H_5Na_3O_7 \cdot 2H_2O$) and toluene were purchased from Beijing Chemical Works (Beijing, China). PEG-SH (MW 5000 Da) was purchased from Aladdin (Shanghai, China). All syntheses progresses were used Ultrapure Milli-Q water. All the glassware was dealed with aqua regia and rinsed with Milli-Q water multiple times, and then dried before use.

Synthesis of the AuNPS. Frens's standard procedure was employed to synthesize the Au NPs.[36] Briefly, 45.5 mL ultrapure water was added to 500 μL chloroauric acid (1%, ω %), and then heated the diluted chloroauric acid to boiling before 500 μL sodium citrate (1%, ω %) was added. After approximately 70 s, the solution changed into brilliant red, and then continued boiling for 30 min to form spherical particles completely. After cooling the mixture solution to room temperature with gentle shook, it was then centrifuged to different volumes of final products (1, 3, and, 6 mL) at 9000 rpm for 5 min and removed the supernatant, and diluted the AuNPs in 350 μL ethanol for next step.

Self-Assembly AuNP Metafilms at the Water−Toluene Interface. First, 20 mg PEG-SH was dissolved in 10 mL ultrapure water and 10 mL toluene separately, and then 30 mg SIS in toluene (contain PEG-SH) was added. Next, 1 mL water (contain PEG-SH) was added to a beaker followed by 800 μL toluene (contain PEG-SH and SIS). There is an obvious interface formed between these two immiscible phases. Then, the ethanol-diluted AuNPs (contain 1, 3, and, 6 mL AuNPs, respectively) in the water−toluene interface were injected by the peristaltic pump with the feeding rate of 0.10 mL/min. The AuNP metafilm was formed while all the ethanol is injected into the interface. Finally, toluene was evaporated at room temperature and then the remaining membrane was peeled off over the water phase, so that we can get an integral film with a brilliant metallic luster.

Fabrication of the SERS Sample. For SERS sensitivity measurement, pieces of the AuNP metafilm were immersed in series of standard CV (from 10^{-7} to 10^{-11} M) and MG (from 10^{-7} to 10^{-11} M) solution for 4 h. For thiram detection, a series of standard thiram solutions of different concentrations (from 1000 to 0.5 ppm) were prepared, and then, the AuNP metafilm was immersed in 0.2 mL thiram solution for 4 h. For thiram detection on the orange pericarp, different concentrations (from 1000 to 0.5 ppm) thiram was sprayed onto small pieces of the orange pericarp, and then wiped with the AuNP metafilm.

Characterization. Field-emission scanning electron microscopy (FE-SEM) was performed on a Jeol-JSM 7500 scanning electron microscope with an accelerating voltage of 5.0 kV. The UV−vis spectrophotometer and fittings were provided by Shimadzu (Japan) Co., Ltd. The mechanical properties of hybrid films were measured under the tensile mode in a universal mechanical testing machine (Shimadzu AGS-X, Japan). Chromatographic analysis was performed with a HPLC instrument (Shimadzu, LC-20A, Japan), which consisted of a waters pump, a reverse-phase C-18 column (Inertsil ODS-SP, 4.6 mm × 150 mm, particle size 5 μm), an ultraviolet detector, and a 20 μL injection loop. The mobile phase was a mixture of methanol and ultrapure water (9:1, v/v), and its flow rate was 1.0 mL min^{-1}. The detection wavelength was set to 272 nm. Zeta-potential measurements were made on Zetasizer Nano ZS90 (Malvern, UK) at 25 °C. Raman spectra were recorded with a JY HR800 Raman spectrometer (HORIBA Jobin Yvon), equipped with a 50× objective (NA = 0.5) and a He−Ne laser with 633 nm wavelength; the laser power values measured in the experiments were obtained from a power meter (0.75 mW at the samples with a spot area of approximately 1.4 μm^2). The Raman band of a silicon wafer at 520.8 cm^{-1} was used to calibrate the spectrometer. The data integration time was 10 s for two accumulations.

RESULTS AND DISCUSSION

Mechanism. Scheme 1 illustrates the procedure of the one-step self-assembly of the flexible AuNP metafilm. A layer with a metallic luster generally appeared at the water−toluene interface while the ethanol-diluted AuNPs were injected, indicating that the AuNPs assembled at the interface.[37] There are two likely causes for this phenomenon: the effects of ethanol and PEG-SH. First, using ethanol to dissolve AuNPs could decrease the surface charge density on the AuNPs because of the displacement of the citrate ions.[19,38] Also, the reduction of the charge density on the AuNPs is the dominant impact for the assembly of the NPs at the water−oil interface.[15,38] On the other hand, the addition of PEG-SH could further adjust the AuNPs' surface charge density.[39] The

DOI: 10.1021/acs.langmuir.8b04271
Langmuir 2019, 35, 4626−4633

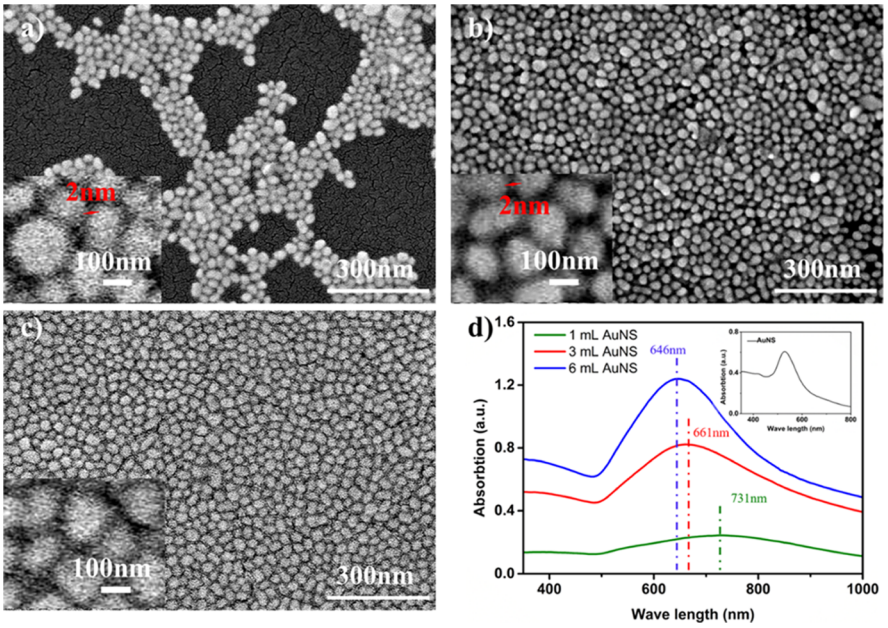

Figure 1. SEM image of the metafilm fabricated with different AuNP solution volumes, (a) 1; (b) 3; and (c) 6 mL, the inset graph shows higher magnification SEM image; (d) UV−vis spectra of the metafilm fabricated with different AuNP solution volumes and the inset graph shows UV−vis spectra of monodispersed AuNPs.

zeta-potential of water, ethanol, and PEG-SH-dispersed AuNPs is shown in Table S1 as −7.1, −2.8, and −1.9 mV, and the zeta-potential decreases with the addition of ethanol and PEG-SH ,verifying the reduction of the AuNPs' surface charge density. The PEG-SH can dissolve both in toluene and water phases because of the hydrophilic and hydrophobic features.[40] Moreover, the PEG-SH can fast cap AuNPs both in toluene and water phases through the strong affinity of thiol groups to the gold surface, which facilitates to stabilize and assemble the NPs at the water−toluene interface.[40−42] Besides, the PEG-SH can also tune the spacing between the gold NPs which will help preventing the NP aggregation.[43]

According to prior studies, the interaction energy among AuNPs can be determined by

$$\phi = \varphi_{vdW}(d_{c-c}) + \varphi_{elec}(d_{c-c}) + \varphi_{ster}(d_{c-c}, l) \quad (1)$$

where the $\varphi_{vdW}(d_{c-c})$, $\varphi_{elec}(d_{c-c})$, and $\varphi_{ster}(d_{c-c},l)$ represent the van der Waals attraction potential, electrostatic repulsion potential, and steric elastic repulsive energy, respectively.[19,38,39,44] In this research, the surface charge density on the gold NPs was adjusted by ethanol and PEG-SH and the remaining surface charge of the gold NPs will redistribute when they are injected in the water−toluene interface until the $\varphi_{vdW}(d_{c-c})$, $\varphi_{elec}(d_{c-c})$, and $\varphi_{ster}(d_{c-c},l)$ reach a new balance, which lead to the formation of an assembly layer of AuNPs at the water−toluene interface.[37,38]

Optical Characterization. The SEM images show the assembled NPs on the metafilm fabricated using different amounts of AuNPs in Figure 1a−c, and the transmission electron microscopy (TEM) image of monodispersed AuNPs is shown in Figure S1 in which the size is 35 nm. While 1 mL of AuNPs was adopted, it was difficult for the NPs to cover the whole SIS film and there were large vacant areas existing, although the NPs were closely arranged, as shown in Figure 1a. As the volume of AuNPs increased to 3 mL, an ordered monolayer film formed on an intact region in Figure 1b, and the average interspace of AuNPs is about 5 nm. By continuously increasing the AuNP amount to 6 mL, the self-assembly metafilm was packed too close to produce effective nanogaps, as shown in Figure 1b. A proper spacing and density of NPs may generate effective "hot spots" which can improve the sensitivity for SERS application.[14,45,46] Moreover, Figure S2a showed the SEM image of the 3 mL AuNP metafilm from the backside, and there were no obvious NPs found in this side which can prove that the NPs stayed at the interface rather than being imbedded into the toluene phase. The thickness of the metafilm was measured in Figure S2b as 44 μm.

Figure 1d shows UV−vis spectra of the metafilm with different quantities of AuNPs being added, in which the peaks of monodispersed AuNPs appear at 528 nm. While the monodispersed NPs were immobilized in the SIS film, the peaks exhibit obvious red-shift because of the electronic coupling interactions between adjacent NPs.[4,7] This shift of plasmon band indicated the formation of the assembled nanostructure which is agreed with the morphology, as shown in SEM images. The surface plasmon absorption was enhanced as the amount of AuNPs increased from 1 to 6 mL. It is noticed that the surface plasmon absorption peaks show blue-shift from 731 to 646 nm between these three kinds of metafilms. It is inferred that the increasement of gold NPs will change the surrounding environment from the polymer film to AuNPs, which may lead to a shift in the SPR peak.[47,48] The shift from 3 to 6 mL is small, verifying that the change in the polymer environment might be the dominant reason for the surface plasmon absorption blue-shift.

More assembled situation under different conditions was investigated and shown in Figure S3. AuNP metafilms fabricated in the toluene phase contain PEG-SH only (Figure S3a), SIS only (Figure S3c), nor PEG-SH or SIS (Figure S3e) while the water phase contains the PEG-SH molecule, and the Figure S3b,d,f demonstrates the same conditions at the toluene phase while the water phase without the PEG-SH molecule. When there is a PEG-SH molecule existed at the water phase, the assembled metafilm showed more perfect monolayer

DOI: 10.1021/acs.langmuir.8b04271
Langmuir 2019, 35, 4626−4633

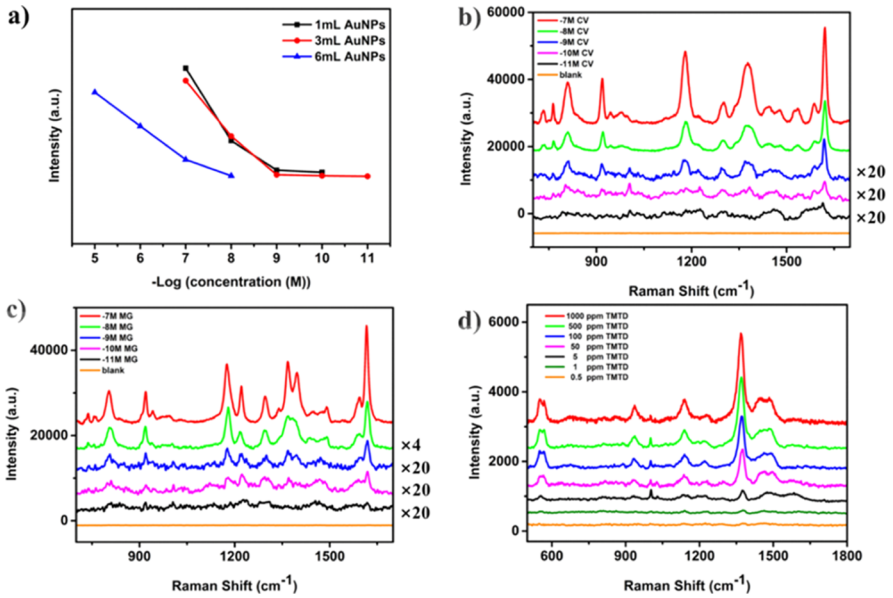

Figure 2. (a) Comparison of SERS intensity at the 1620 cm^{-1} peak of different amounts of AuNP-fabricated metafilms adsorbing different concentrations of CV standard samples (black line: 1 mL AuNPs; red line: 3 mL AuNPs; blue line: 6 mL AuNPs); (b) SERS spectra of the 3 mL AuNP metafilm adsorbing different concentrations of CV standard samples from 10^{-7} to 10^{-11} M (red line: 10^{-7} M; green line: 10^{-8} M; blue line: 10^{-9} M; pink line: 10^{-10} M; black line: 10^{-11} M; orange line: blank); (c) SERS spectra of the 3 mL AuNP metafilm adsorbing different concentrations of MG standard samples from 10^{-7} to 10^{-11} M (red line: 10^{-7} M; green line: 10^{-8} M; blue line: 10^{-9} M; pink line: 10^{-10} M; black line: 10^{-11} M; orange line: blank); and (d) SERS spectra of the 3 mL AuNP metafilm adsorbing different concentrations of thiram standard samples from 1000 to 0.5 ppm.

structures compared with the corresponding conditions without PEG-SH molecules, in which the multilayer structures were preferred. Meanwhile, if compared Figure S3c with (a,e), we can find that the existence of the SIS molecule can introduce more NP coverage ratios while there are more void areas in the absence of SIS. The results reveal that the PEG-SH molecule at water and toluene phases is a crucial factor to produce uniform monolayer nanostructures at two liquid interfaces, and the SIS molecule can help offer more effective assembled area. The tensile stress−strain curves of the 3 mL AuNP metafilm are shown in Figure S4, and the metafilm has a large elastic deformation with a high strain ratio reaching 1796%, which demonstrates excellent tenacity of this film. The outstanding elasticity of the metafilm provides a platform for direct analysis on the uneven surface which indicates further application potential.

SERS Performance. The ordered self-assembled AuNP metafilm was employed in SERS measurement as shown in Figures 2 and S5. Using CV as the SERS probe, the lowest detect concentration of 1, 3, and 6 mL AuNP metafilms is 10^{-10}, 10^{-11}, and 10^{-8} M (Figure 2a), respectively. The SERS spectra are shown in Figures 2b and S5. Hence, the 3 mL AuNP metafilm was selected for SERS measurement using MG as the probe and the limit of detection as low as 10^{-11} M, similarly (Figure 2c). Five major characteristic peaks could be observed in Figure 2b at 809, 918, 1180, 1378, and 1620 cm^{-1}, which are assigned to out-of-plane phenyl−H bending, ring-breathing, in-plane aromatic C−H vibration, in-plane N−phenyl stretching vibration, and in-plane C−C stretching vibration of the ring, respectively.[49,50] In Figure 2c, the peaks at 805, 918, 1178, 1370, and 1618 cm^{-1} are same to the CV because of the similar structures. Also, the peaks at 1220 and 1396 cm^{-1} are corresponding to C−H ring in-plane bending vibrations and C−H ring in-plane bending, respectively.[49−51]

Furthermore, the 3 mL AuNP metafilm was used to detect trace thiram (TMTD), a dithiocarbamate fungicide widely applied to prevent crop damage in the field.[52−54] Figure 2d shows the Raman spectra of TMTD standard samples with different concentrations from 1000 to 0.5 ppm, using the 3 mL AuNP metafilm as the SERS substrate. The stretching CH_3N and C═S vibration modes appear at 926 cm^{-1}, peak at 1140 cm^{-1} belong to CN stretching vibrations and rocking CH_3 mode, and the peak of 1375 cm^{-1} is assigned to the CN stretching mode and symmetric CH_3 deformation mode.[53,55] It can be seen that the lowest TMTD detection concentration on this metafilm is 0.5 ppm, which is below the maximal residue limit of 5 ppm in fruit according to National Standard of China (GB 2763-2016). A favorable linearity relation is shown in Figure S6, demonstrating the quantitative characteristic of this SERS substrate.

The main limitation of the 1 mL AuNP metafilm's SERS sensitivity is the amount of AuNPs. The existence of large vacant areas as we can see in SEM images reduces the effective area for SERS enhancement. However, the 6 mL AuNP metafilm shows nonideal SERS performance as the NPs presented overspread and closed packed. This inconsistency may be because there are limited effective space for probe molecules to adsorb.[34,35] In conclusion, the satisfactory detection level of the 3 mL AuNP metafilm attributes to the large region of the uniformly assembled nanostructure which can supply abundant number of "hot spots" and the reasonable nanogaps that maintain the analyte molecules feasible to enter into and adsorbed.

The Raman enhancement factor (EF) was calculated to evaluate the SERS activity by employing the formula

$$EF = \frac{I_{SERS}}{I_{NRS}} \times \frac{C_{NRS}}{C_{SERS}} \quad (2)$$

DOI: 10.1021/acs.langmuir.8b04271
Langmuir 2019, 35, 4626−4633

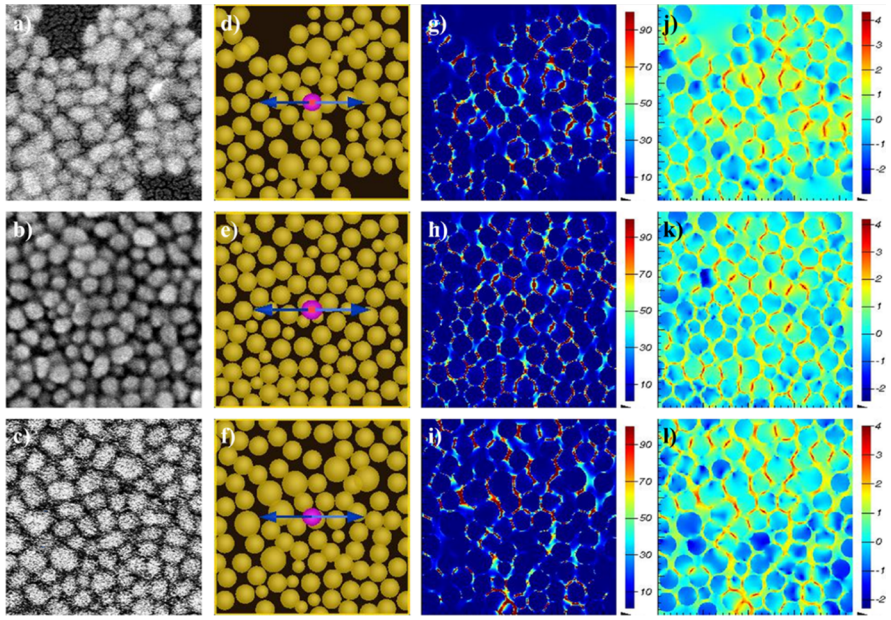

Figure 3. 3D-FDTD model (sphere) for AuNP aggregation on the metafilm fabricated with different AuNP solution volumes according to SEM images (a–c): 1 (a,d); 3 (b,e); and 6 mL (c,f). 2D patterns of E-field intensity amplitude ($|E|^2$) around the corresponding model (g–l). *XY* planes containing geometric centers of the body structure were normal-plotted with the scale bar of 100 (g–i) and log-plotted (j–l).

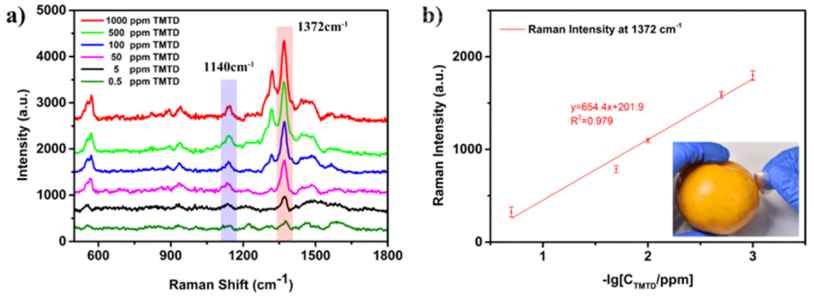

Figure 4. (a) SERS spectra of thiram (from 1000 to 0.5 ppm) adsorbed on the orange surface, acquired by swabbing the orange surface with the AuNP metafilm; (b) Raman intensity at 1372 cm^{-1} vs the negative logarithms of the thiram concentrations ranging from 1000 to 0.5 ppm.

where I_{SERS} and C_{SERS} are normalized Raman peak intensities and the concentration of the reporter molecule chemisorbed on the SERS substrate; I_{NRS} and C_{NRS} are same parameters that in the reference solution.[56−58] The CV concentration is 10^{-11} M on the SERS substrate and 10^{-3} M in the reference solution, and the MG concentration is 10^{-11} M on the SERS substrate and 10^{-3} M in the reference solution. The EF was calculated to be 3.4×10^7 according to peaks at 1620 cm^{-1} with CV as the probe. By using MG as the probe, the EF was calculated to be 1×10^7, according to peaks at 1618 cm^{-1}, (corresponding SERS spectra are provided in Supporting Information Figure S7).

Finite-Difference Time Domain (FDTD) Calculations. The 3D-finite difference time domain (FDTD) method was introduced to further understand the electromagnetic enhancement effect on the surface of substrates. E-field distribution was calculated by numerically solving Maxwell's differential equations. The 3D-FDTD model (sphere) for NPs aggregation was built with spheres. The diameters are 20, 30, and 40 nm. Distribution of AuNP aggregation was designed according to SEM images. For comparison, calculation results of island models were also provided as shown in Figure S8. The excitation source with 633 nm wavelength. The refractive index of the gold material is from Johnson and Christy data.[59] The calculated electric field intensity ($|E|^2$) of the AuNP aggregation is shown in Figure 3. Considering that the spectral enhancement in SERS varied as the fourth power of local field enhancement of substrates. The maximum EF ($|E|^4$) could reach a value of 10^8. In general, the region with maximum enhancement accounts for less than 1% of the whole substrate surface, thus average enhancement along with chemical enhancement could be approximately estimated to be 6−7 order of magnitudes, which agrees well with the experimental results. Results on aggregation on the metafilm with 1 and 3 mL AuNP solutions indicated larger enhancement compared to that with 6 mL AuNP solution. The maximum E-field intensity amplitude ($|E|^2$) around the 3D-FDTD model (sphere) for AuNP aggregation on the metafilm fabricated with different AuNP solution volumes was shown in Figure S9 with the result of 2.3×10^4 (1 mL), 1.6×10^4 (3 mL), and 1×10^4 (6 mL). However, the large vacant areas reduce the effective area for SERS enhancement of the 1 mL AuNP metafilm, although the calculation result shows the highest $|E|^2$. Furthermore, more hot spots in aggregation might contribute to better SERS results for the metafilm fabricated with 3 mL AuNP solution.

Application as the Flexible SERS Substrate. The high sensitivity and good quantitative examination make this flexible

DOI: 10.1021/acs.langmuir.8b04271
Langmuir 2019, 35, 4626−4633

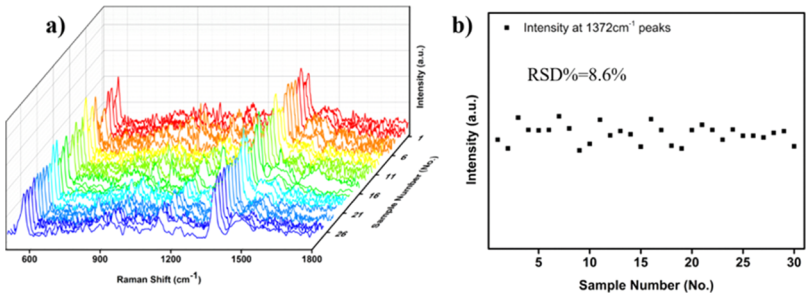

Figure 5. (a) SERS spectra collected from thirty random points on metafilm substrates that have been soaked in 5 ppm TMTD for 4 h; (b) corresponding RSD results of (a) calculated by SERS intensities for 1372 cm^{-1} Raman peaks.

AuNP metafilm a promising SERS substrate to probe the residual molecules on various surfaces. The obtained flexible metafilm SERS substrate carried out a realistic SERS detection to prove the practicability. The orange pericarp was sprayed by ethanol-dissolved thiram, and swabbed the flexible metafilm on it directly. As shown in Figure 4a, obvious characteristic peaks could be observed, and the peak at 1372 cm^{-1} still can be distinguished even with TMTD concentration as low as 0.5 ppm, verifying the reliability of the one-step assembling metafilm in practical detection. Quantitative analysis of thiram was achieved at peaks for 1372 cm^{-1} from 1000 to 0.5 ppm, which satisfied the linear relationship of $y = 654.4x + 201.9$ with a correlation coefficient of 0.979 in Figure 4b. Furthermore, there is no obvious signal found in the orange surface without TMTD treatment, which was detected by swabbing the surface with the AuNP flexible metafilm, as shown in the Figure S10, further demonstrating the advantages in practical applications. High-performance liquid chromatography (HPLC) was adopted to validate the SERS method, Figure S11 shows 0.5 ppm TMTD detected by SERS and HPLC. The result indicates the accuracy of SERS detection based on this metafilm and the high sensitivity makes this film a promising substrate for practical food safety detection.

SERS Reproducibility of the AuNP Metafilm. To measure the SERS reproducibility of the flexible substrate, we collected SERS spectra of thirty random points of the 5 ppm TMTD-soaked metafilm, which is displayed in Figure 5a. The signal intensity distribution at 1372 cm^{-1} is shown in Figure 5b with the intensity variation of 8.6%. The SERS spectra collected from five difference batches of the fabricated metafilm are shown in Figure S12, in which the relative standard deviation (RSD) % is 9.9% for peaks of 1372 cm^{-1}, and this result implies a good homogeneity of the substrate.

SUMMARY AND CONCLUSIONS

We have developed a one-step method for the first time to prepare the flexible SERS metafilm with self-assembled gold NPs at the water−toluene interface for detecting trace thiram on the orange pericarp. The self-assembled gold NP metafilm fabricated at the water−toluene interface was verified with advantages of high uniformity and close packing. The sensitivity of the SERS substrate was proved by the Raman test on CV and MG with a minimum detection concentration of 1×10^{-11} and 1×10^{-11} M. The high sensitivity and flexibility make the self-assembled gold NP metafilm a promising substrate for practical food safety detection. The detection concentration for thiram on the orange pericarp could reach 1×10^{-6} M, which is much lower than GB demand. The present study raises the possibility of fabricating self-assembled nanostructures at the liquid−liquid interface without a transfer procedure, which contributes to further application in practical trace SERS detection.

ASSOCIATED CONTENT

Supporting Information

The Supporting Information is available free of charge on the ACS Publications website at DOI: 10.1021/acs.langmuir.8b04271.

TEM images of monodispersed AuNPs, SEM image of backside of the 3 mL AuNP metafilm and different fabricated assembled results, tensile stress−strain curves and thickness of the 3 mL AuNP metafilm, corresponding SERS spectra for EF calculation, comparation of SERS spectra under different thiram treatment conditions, HPLC detection result, RSD for different metafilms, and zeta-potential of different solvent-dissolved AuNPs (PDF)

AUTHOR INFORMATION

Corresponding Authors

*E-mail: youtt@buaa.edu.cn (T.Y.).
*E-mail: pgyin@buaa.edu.cn (P.Y.).

ORCID

Penggang Yin: 0000-0001-6796-5921

Notes

The authors declare no competing financial interest.

ACKNOWLEDGMENTS

This work was supported by the National Natural Science Foundation of China (51572009 and 51872011).

REFERENCES

(1) Shi, S.; Russell, T. P. Nanoparticle Assembly at Liquid-Liquid Interfaces: From the Nanoscale to Mesoscale. *Adv. Mater.* **2018**, *30*, No. e1800714.

(2) Guo, Q.; Xu, M.; Yuan, Y.; Gu, R.; Yao, J. Self-Assembled Large-Scale Monolayer of Au Nanoparticles at the Air/Water Interface Used as a SERS Substrate. *Langmuir* **2016**, *32*, 4530−4537.

(3) Kim, B.; Tripp, S. L.; Wei, A. Self-organization of large gold nanoparticle arrays. *J. Am. Chem. Soc.* **2001**, *123*, 7955−7956.

(4) Huang, T.; Meng, F.; Qi, L. Facile Synthesis and One-Dimensional Assembly of Cyclodextrin-Capped Gold Nanoparticles and Their Applications in Catalysis and Surface-Enhanced Raman Scattering. *J. Phys. Chem. C* **2009**, *113*, 13636−13642.

(5) Huang, X.; Li, M.; Green, D. C.; Williams, D. S.; Patil, A. J.; Mann, S., Interfacial assembly of protein-polymer nano-conjugates into stimulus-responsive biomimetic protocells. *Nat. Commun.* **2013**, *4*, DOI: 10.1038/ncomms3239.

DOI: 10.1021/acs.langmuir.8b04271
Langmuir 2019, 35, 4626−4633

(6) Brust, M.; Bethell, D.; Kiely, C. J.; Schiffrin, D. J. Self-Assembled Gold Nanoparticle Thin Films with Nonmetallic Optical and Electronic Properties. *Langmuir* **1998**, *14*, 5425−5429.
(7) Chen, S. Langmuir−Blodgett Fabrication of Two-Dimensional Robust Cross-Linked Nanoparticle Assemblies. *Langmuir* **2001**, *17*, 2878−2884.
(8) Guo, Q.; Teng, X.; Rahman, S.; Yang, H. Patterned Langmuir−Blodgett Films of Monodisperse Nanoparticles of Iron Oxide Using Soft Lithography. *J. Am. Chem. Soc.* **2003**, *125*, 630−631.
(9) Heath, J. R.; Knobler, C. M.; Leff, D. V. Pressure/Temperature Phase Diagrams and Superlattices of Organically Functionalized Metal Nanocrystal Monolayers: The Influence of Particle Size, Size Distribution, and Surface Passivant. *J. Phys. Chem. B* **1997**, *101*, 189−197.
(10) Mahmoud, M. A.; Tabor, C. E.; El-Sayed, M. A. Surface-Enhanced Raman Scattering Enhancement by Aggregated Silver Nanocube Monolayers Assembled by the Langmuir−Blodgett Technique at Different Surface Pressures. *J. Phys. Chem. C* **2009**, *113*, 5493−5501.
(11) Hatab, N. A.; Hsueh, C.-H.; Gaddis, A. L.; Retterer, S. T.; Li, J.-H.; Eres, G.; Zhang, Z.; Gu, B. Free-Standing Optical Gold Bowtie Nanoantenna with Variable Gap Size for Enhanced Raman Spectroscopy. *Nano Lett.* **2010**, *10*, 4952−4955.
(12) Haynes, C. L.; Van Duyne, R. P. Nanosphere lithography: A versatile nanofabrication tool for studies of size-dependent nanoparticle optics. *J. Phys. Chem. B* **2001**, *105*, 5599−5611.
(13) Giersig, M.; Mulvaney, P. Preparation of ordered colloid monolayers by electrophoretic deposition. *Langmuir* **1993**, *9*, 3408−3413.
(14) Prusková, M.; Sutrová, V.; Šlouf, M.; Vlčková, B.; Vohlídal, J.; Šloufová, I. Arrays of Ag and Au Nanoparticles with Terpyridine- and Thiophene-Based Ligands: Morphology and Optical Responses. *Langmuir* **2017**, *33*, 4146−4156.
(15) Wang, M.; Zhang, Z.; He, J. A SERS Study on the Assembly Behavior of Gold Nanoparticles at the Oil/Water Interface. *Langmuir* **2015**, *31*, 12911−12919.
(16) Liu, H.; Yang, Z.; Meng, L.; Sun, Y.; Wang, J.; Yang, L.; Liu, J.; Tian, Z. Three-Dimensional and Time-Ordered Surface-Enhanced Raman Scattering Hotspot Matrix. *J. Am. Chem. Soc.* **2014**, *136*, 5332−5341.
(17) Liu, R.; Li, S.; Liu, J.-F. Self-assembly of plasmonic nanostructures into superlattices for surface-enhanced Raman scattering applications. *Trac. Trends Anal. Chem.* **2017**, *97*, 188−200.
(18) Zhang, Y.-R.; Xu, Y.-Z.; Xia, Y.; Huang, W.; Liu, F.-A.; Yang, Y.-C.; Li, Z.-L. A novel strategy to assemble colloidal gold nanoparticles at the water-air interface by the vapor of formic acid. *J. Colloid Interface Sci.* **2011**, *359*, 536−541.
(19) Hu, L.; Chen, M.; Fang, X.; Wu, L. Oil-water interfacial self-assembly: a novel strategy for nanofilm and nanodevice fabrication. *Chem. Soc. Rev.* **2012**, *41*, 1350−1362.
(20) He, S.; Yao, J.; Jiang, P.; Shi, D.; Zhang, H.; Xie, S.; Pang, S.; Gao, H. Formation of silver nanoparticles and self-assembled two-dimensional ordered superlattice. *Langmuir* **2001**, *17*, 1571−1575.
(21) Liu, J.-W.; Zhang, S.-Y.; Qi, H.; Wen, W.-C.; Yu, S.-H. A General Strategy for Self-Assembly of Nanosized Building Blocks on Liquid/Liquid Interfaces. *Small* **2012**, *8*, 2412−2420.
(22) Moskovits, M. Surface-enhanced Raman spectroscopy: a brief retrospective. *J. Raman Spectrosc.* **2005**, *36*, 485−496.
(23) Stiles, P. L.; Dieringer, J. A.; Shah, N. C.; Van Duyne, R. P. Surface-Enhanced Raman Spectroscopy. *Annu. Rev. Anal. Chem.* **2008**, *1*, 601−626.
(24) Nie, S. Probing single molecules and single nanoparticles by surface-enhanced Raman scattering. *Science* **1997**, *275*, 1102.
(25) Prawer, S.; Nemanich, R. J. Raman spectroscopy of diamond and doped diamond. *Philos. Trans. R. Soc., A* **2004**, *362*, 2537−2565.
(26) Porter, M. D.; Lipert, R. J.; Siperko, L. M.; Wang, G.; Narayanan, R. SERS as a bioassay platform: fundamentals, design, and applications. *Chem. Soc. Rev.* **2008**, *37*, 1001−1011.
(27) Alvarez-Puebla, R. A.; Liz-Marzán, L. M. SERS-Based Diagnosis and Biodetection. *Small* **2010**, *6*, 604−610.
(28) Doering, W. E.; Nie, S. Single-molecule and single-nanoparticle SERS: Examining the roles of surface active sites and chemical enhancement. *J. Phys. Chem. B* **2002**, *106*, 311−317.
(29) Halvorson, R. A.; Vikesland, P. J. Surface-Enhanced Raman Spectroscopy (SERS) for Environmental Analyses. *Environ. Sci. Technol.* **2010**, *44*, 7749−7755.
(30) Li, P.; Dong, R.; Wu, Y.; Liu, H.; Kong, L.; Yang, L. Polystyrene/Ag nanoparticles as dynamic surface-enhanced Raman spectroscopy substrates for sensitive detection of organophosphorus pesticides. *Talanta* **2014**, *127*, 269−275.
(31) Dong, R.; Weng, S.; Yang, L.; Liu, J. Detection and Direct Readout of Drugs in Human Urine Using Dynamic Surface-Enhanced Raman Spectroscopy and Support Vector Machines. *Anal. Chem.* **2015**, *87*, 2937−2944.
(32) Li, K.; Zhang, N.; Zhang, T.; Wang, Z.; Chen, M.; Wu, T.; Ma, S.; Zhang, M.; Zhang, J.; S, D. U.; Shum, P. P.; Olivo, M.; Wei, L. Formation of ultra-flexible, conformal, and nano-patterned photonic surfaces via polymer cold-drawing. *J. Mater. Chem. C* **2018**, *6*, 4649−4657.
(33) Liu, H.; Yang, Z.; Meng, L.; Sun, Y.; Wang, J.; Yang, L.; Liu, J.; Tian, Z. Three-Dimensional and Time-Ordered Surface-Enhanced Raman Scattering Hotspot Matrix. *J. Am. Chem. Soc.* **2014**, *136*, 5332−5341.
(34) Ma, Y.; Liu, H.; Mao, M.; Meng, J.; Yang, L.; Liu, J. Surface-Enhanced Raman Spectroscopy on Liquid Interfacial Nanoparticle Arrays for Multiplex Detecting Drugs in Urine. *Anal. Chem.* **2016**, *88*, 8145−8151.
(35) Tian, L.; Su, M.; Yu, F.; Xu, Y.; Li, X.; Li, L.; Liu, H.; Tan, W. Liquid-state quantitative SERS analyzer on self-ordered metal liquid-like plasmonic arrays. *Nat. Commun.* **2018**, *9*, 3642.
(36) Frens, G. Controlled Nucleation for the Regulation of the Particle Size in Monodisperse Gold Suspensions. *Nat. Phys. Sci.* **1973**, *241*, 20−22.
(37) Yang, G.; Hallinan, D. T. Self-assembly of large-scale crack-free gold nanoparticle films using a 'drain-to-deposit' strategy. *Nanotechnology* **2016**, *27*, 225604−225614.
(38) Reincke, F.; Hickey, S. G.; Kegel, W. K.; Vanmaekelbergh, D. Spontaneous assembly of a monolayer of charged gold nanocrystals at the water/oil interface. *Angew. Chem. Int. Ed.* **2004**, *43*, 458−462.
(39) Du, Y.; Wei, W.; Zhang, X.; Li, Y. Tuning Metamaterials Nanostructure of Janus Gold Nanoparticle Film for Surface-Enhanced Raman Scattering. *J. Phys. Chem. C* **2018**, *122*, 7997−8002.
(40) Alkilany, A. M.; Yaseen, A. I. B.; Park, J.; Eller, J. R.; Murphy, C. J. Facile phase transfer of gold nanoparticles from aqueous solution to organic solvents with thiolated poly(ethylene glycol). *RSC Adv.* **2014**, *4*, 52676−52679.
(41) Lee, M.-J.; Lim, S.-H.; Ha, J.-M.; Choi, S.-M. Green Synthesis of High-Purity Mesoporous Gold Sponges Using Self-Assembly of Gold Nanoparticles Induced by Thiolated Poly(ethylene glycol). *Langmuir* **2016**, *32*, 5937−5945.
(42) Zhang, S.-Y.; Regulacio, M. D.; Han, M.-Y. Self-assembly of colloidal one-dimensional nanocrystals. *Chem. Soc. Rev.* **2014**, *43*, 2301−2323.
(43) Karakoti, A. S.; Das, S.; Thevuthasan, S.; Seal, S. PEGylated Inorganic Nanoparticles. *Angew. Chem.* **2011**, *50*, 1980−1994.
(44) Reincke, F.; Kegel, W. K.; Zhang, H.; Nolte, M.; Wang, D.; Vanmaekelbergh, D.; Möhwald, H. Understanding the self-assembly of charged nanoparticles at the water/oil interface. *Phys. Chem. Chem. Phys.* **2006**, *8*, 3828−3835.
(45) Gittins, D. I.; Susha, A. S.; Schoeler, B.; Caruso, F. Dense nanoparticulate thin films via gold nanoparticle self-assembly. *Adv. Mater.* **2002**, *14*, 508−512.
(46) Yockell-Lelièvre, H.; Lussier, F.; Masson, J.-F. Influence of the Particle Shape and Density of Self-Assembled Gold Nanoparticle Sensors on LSPR and SERS. *J. Phys. Chem. C* **2015**, *119*, 28577−28585.

DOI: 10.1021/acs.langmuir.8b04271
Langmuir 2019, 35, 4626−4633

(47) Setoura, K.; Werner, D.; Hashimoto, S. Optical Scattering Spectral Thermometry and Refractometry of a Single Gold Nanoparticle under CW Laser Excitation. *J. Phys. Chem. C* **2012**, *116*, 15458−15466.
(48) Driskell, J. D.; Lipert, R. J.; Porter, M. D. Labeled gold nanoparticles immobilized at smooth metallic substrates: Systematic investigation of surface plasmon resonance and surface-enhanced Raman scattering. *J. Phys. Chem. B* **2006**, *110*, 17444−17451.
(49) Song, J.; Huang, Y.; Fan, Y.; Zhao, Z.; Yu, W.; Rasco, B.; Lai, K. Detection of Prohibited Fish Drugs Using Silver Nanowires as Substrate for Surface-Enhanced Raman Scattering. *Nanomaterials* **2016**, *6*, 175.
(50) Pei, L.; Huang, Y.; Li, C.; Zhang, Y.; Rasco, B. A.; Lai, K. Detection of Triphenylmethane Drugs in Fish Muscle by Surface-Enhanced Raman Spectroscopy Coupled with Au-Ag Core-Shell Nanoparticles. *J. Nanomater.* **2014**, *2014*, 730915.
(51) Xiao, G.; Li, Y.; Shi, W.; Shen, L.; Chen, Q.; Huang, L. Highly sensitive, reproducible and stable SERS substrate based on reduced graphene oxide/silver nanoparticles coated weighing paper. *Appl. Surf. Sci.* **2017**, *404*, 334−341.
(52) Kang, J. S.; Hwang, S. Y.; Lee, C. J.; Lee, M. S. SERS of dithiocarbamate pesticides adsorbed on silver surface; Thiram. *Bull. Korean Chem. Soc.* **2002**, *23*, 1604−1610.
(53) Liu, B.; Han, G.; Zhang, Z.; Liu, R.; Jiang, C.; Wang, S.; Han, M.-Y. Shell Thickness-Dependent Raman Enhancement for Rapid Identification and Detection of Pesticide Residues at Fruit Peels. *Anal. Chem.* **2012**, *84*, 255−261.
(54) Sharma, V. K.; Aulakh, J. S.; Malik, A. K. Thiram: degradation, applications and analytical methods. *Journal Of Environmental Monitoring* **2003**, *5*, 717−723.
(55) Liang, X.; Wang, Y.-S.; You, T.-T.; Zhang, X.-J.; Yang, N.; Wang, G.-S.; Yin, P.-G. Interfacial synthesis of a three-dimensional hierarchical MoS2-NS@Ag-NP nanocomposite as a SERS nanosensor for ultrasensitive thiram detection. *Nanoscale* **2017**, *9*, 8879−8888.
(56) K, J.; S, B.; Ganiga, M.; R, D.; S, A.; Cyriac, J.; George, B. K. Effective SERS detection using a flexible wiping substrate based on electrospun polystyrene nanofibers. *Anal. Methods* **2017**, *9*, 3998−4003.
(57) Jia, H.; Zeng, J.; Song, W.; An, J.; Zhao, B. Preparation of silver nanoparticles by photo-reduction for surface-enhanced Raman scattering. *Thin Solid Films* **2006**, *496*, 281−287.
(58) Webb, J. A.; Aufrecht, J.; Hungerford, C.; Bardhan, R. Ultrasensitive analyte detection with plasmonic paper dipsticks and swabs integrated with branched nanoantennas. *J. Mater. Chem. C* **2014**, *2*, 10446−10454.
(59) Johnson, P. B.; Christy, R. W. Optical Constants of the Noble Metals. *Phys. Rev. B: Solid State* **1972**, *6*, 4370−4379.

DOI: 10.1021/acs.langmuir.8b04271
Langmuir 2019, 35, 4626−4633